Single production of an exotic vector-like Y quark at future high energy pp colliders

Liangliang Shang[1,2*], Yuxiao Yan[1†], Stefano Moretti[2,3‡], Bingfang Yang[1§]

[1] *School of Physics, Henan Normal University, Xinxiang 453007, PR China*

[2] *Department of Physics and Astronomy,*

Uppsala University, Box 516, SE-751 20 Uppsala, Sweden

[3] *School of Physics and Astronomy, University of Southampton,*

Highfield, Southampton SO17 1BJ, UK

Abstract

Vector-like quarks have been predicted in various new physics scenarios beyond the Standard Model (SM). In a simplified modelling of a (B, Y) doublet including a vector-like quark Y, with charge $-\frac{4}{3}$e, there are only two free parameters: the Y coupling κ_Y and mass m_Y. In the five flavor scheme, we investigate the single production of the Y state decaying into Wb at the Large Hadron Collider (LHC) Run-III and High-Luminosity LHC (HL-LHC) operating at $\sqrt{s}$ = 14 TeV, the possible High-Energy LHC (HE-LHC) with $\sqrt{s}$ = 27 TeV as well as the Future Circular Collider in hadron-hadron mode (FCC-hh) with $\sqrt{s}$ = 100 TeV. Through detailed signal-to-background analyses and detector simulations, we assess the exclusion capabilities of the Y state at the different colliders. We find that this can be improved significantly with increasing collision energy, especially at the HE-LHC and FCC-hh, both demonstrating an obvious advantage with respect to the HL-LHC case in the case of high m_Y. Assuming a 10% systematic uncertainty on the background event rate, the exclusion capabilities are summarized as follows: (1) the LHC Run-III can exclude the correlated regions of $\kappa_Y \in [0.044, 0.5]$ and $m_Y \in [1000\ \text{GeV}, 3099\ \text{GeV}]$ with integrated luminosity $L = 300\ \text{fb}^{-1}$; (2) the HL-LHC can exclude the correlated regions of $\kappa_Y \in [0.027, 0.5]$ and $m_Y \in [1000\ \text{GeV}, 3653\ \text{GeV}]$ with $L = 3\ \text{ab}^{-1}$; (3) the HE-LHC can exclude the correlated regions of $\kappa_Y \in [0.030, 0.5]$ and $m_Y \in [1000\ \text{GeV}, 4936\ \text{GeV}]$ with $L = 3\ \text{ab}^{-1}$; (4) the FCC-hh can exclude the correlated regions of $\kappa_Y \in [0.051, 0.5]$ and $m_Y \in [1000\ \text{GeV}, 6610\ \text{GeV}]$ with $L = 3\ \text{ab}^{-1}$.

* Email: shangliangliang@htu.edu.cn; liangliang.shang@physics.uu.se

† Email: yanyuxiao@stu.htu.edu.cn

‡ Email: s.moretti@soton.ac.uk; stefano.moretti@physics.uu.se

§ E-mail: yangbingfang@htu.edu.cn

I. INTRODUCTION

In 2012, the ATLAS and CMS experiments at the Large Hadron Collider (LHC) made a significant discovery by confirming the existence of the Higgs boson, thereby providing further validation for the Standard Model (SM) [1, 2]. However, the SM has certain limits in addressing several prominent issues, such as neutrino masses, gauge hierarchy, dark matter and dark energy. In various new physics scenarios like little Higgs models [3–6], extra dimensions [7], composite Higgs models [8–13] and other extended models [14–16], Vector-Like Quarks (VLQs) are predicted to play a role in resolving the gauge hierarchy problem by mitigating the quadratic divergences of the Higgs field. Such VLQs are fermions with spin $\frac{1}{2}$ and possess the unique characteristic of undergoing both left- and right-handed component transformations under the Electro-Weak (EW) symmetry group of the SM [17]. Unlike chiral quarks, VLQs do not acquire masses through Yukawa couplings to the Higgs field and therefore have the potential to counterbalance loop corrections to the Higgs boson mass stemming from the top quark of the SM. Furthermore, VLQs can generate characteristic signatures at colliders and have been widely studied (see, for example, [18–20, 20–53]).

A VLQ model typically introduces four new states: T, B, X and Y, their electric charges being $+\frac{2}{3}$, $-\frac{1}{3}$, $+\frac{5}{3}$ and $-\frac{4}{3}$, respectively. In such kind of model, VLQs can be categorized into three types: singlets (T), (B), doublets (X,T), (T,B), (B,Y) and triplets (X,T,B), (T,B,Y). Notably, the Y quark cannot exist as a singlet. Further, it is expected to decay with a 100% Branching Ratio (BR) into a b quark and W boson when Y is lighter than the other VLQs, whether in a doublet or triplet.

In this study, we will focus on the observability of single Y production at the Large Hadron Collider (LHC) Run-III, the High-Luminosity LHC (HL-LHC) [54, 55], the High-Energy LHC (HE-LHC) [56] and the Future Circular Collider operating in hadron-hadron mode (FCC-hh) [57], specifically, within the (B,Y) doublet realisation.

The ATLAS Collaboration conducted a search for a VLQ Y at 13 TeV with an integrated luminosity of 36.1 fb^{-1} [58]. They found that the upper limits on the mixing angle are as small as $|\sin\theta_R| = 0.17$ for a Y quark with a mass of 800 GeV in the (B,Y) doublet model, and $|\sin\theta_L| = 0.16$ for a Y quark with a mass of 800 GeV in the (T,B,Y) triplet model. The CMS Collaboration also conducted a search for Y states in the Wb channel

at 13 TeV using 2.3 fb^{-1} of data [59]. They searched for final states involving one electron or muon, at least one b-tagged jet with large transverse momentum, at least one jet in the forward region of the detector plus (sizeable) missing transverse momentum. Their findings indicate that the observed (expected) lower mass limits are 1.40 (1.0) TeV for a VLQ Y with a coupling value of 0.5 and a BR($Y \to W^- b$) = 1. The ATLAS Collaboration recently presented a search for the pair-production of VLQ T in the lepton+jets final state using 140 fb^{-1} at 13 TeV [60]. They pointed out that the most stringent limits are set for the scenario BR($T \to W^+ b$)= 1, for which T masses below 1700 GeV (1570 GeV) are observed (expected) to be excluded at 95% Confidence Level (CL). And the limits can also apply to a VLQ Y with BR($Y \to W^- b$)= 1. All such limits stem from VLQ pair production, induced by Quantum Chromo-Dynamics (QCD).

Furthermore, there are comparable exclusion limits on the mixing parameter $\sin\theta_R$ from EW Precision Observables (EWPOs), for example within the (B, Y) doublet model, Ref. [17] found that the upper limits on $\sin\theta_R$ are approximately 0.21 and 0.15 at m_Y = 1000 GeV and 2000 GeV respectively at 95% CL from the oblique parameters S and T. Ref. [61] highlighted that, considering the W boson mass measurement by the CDF collaboration [62], the 2σ bounds on $\sin\theta_R$ from the oblique parameters S, T and U are approximately $[0.15, 0.23]$ and $[0.09, 0.13]$ at m_Y = 1000 GeV and 3000 GeV in a conservative average scenario, respectively. They also pointed out that the constraints from the $Zb\bar{b}$ coupling are weaker than those from the EWPOs for about $m_Y > 1600$ GeV.

The single production of a VLQ is instead model dependent, as the couplings involved are EW ones, yet they may make a significant contribution to the total VLQ production cross section, compared to the pair production, due to less phase space suppression, in the region of high VLQ masses. In this work, we will in particular focus on the process $pp \to Y(\to W^- b)\bar{b}j \to l^- \bar{\nu}_l b\bar{b}j$ (with l^- standing for electron or muon and j standing for first two-generation quark jets), combined with its charged conjugated process $pp \to \bar{Y}bj$. We expect that the forthcoming results will provide complementary information to the one provided by VLQ pair production in the quest to detect a doublet Y quark at the aforementioned future colliders.

The paper is structured as follows. In Section II, we introduce the simplified VLQ model used in our simulations. In Section III, we analyze the properties of the signal

process and SM backgrounds. Subsequently, we conduct simulations and calculate the Y state exclusion and discovery capabilities at the HL-LHC, HE-LHC and FCC-hh. Finally, in Section IV, we provide a summary. (We also have an Appendix where we map the Y state of our simplified model onto the (B, Y) doublet representation.)

II. DOUBLET Y VLQ IN A SIMPLIFIED MODEL

As mentioned, in a generic VLQ model, one can include four types of states called T, B, X and Y, with electric charges $+\frac{2}{3}$, $-\frac{1}{3}$, $+\frac{5}{3}$ and $-\frac{4}{3}$, respectively. Under the SM gauge group, $SU(3)_C \times SU(2)_L \times U(1)_Y$, there are seven possible representations of VLQs as shown in Table I.

	T	B	(T,B)	(B,Y)	(X,T)	(T,B,Y)	(X,T,B)
$SU(3)_C$	3	3	3	3	3	3	3
$SU(2)_L$	1	1	2	2	2	3	3
$U(1)_Y$	$\frac{2}{3}$	$-\frac{1}{3}$	$\frac{1}{6}$	$-\frac{5}{6}$	$\frac{7}{6}$	$-\frac{1}{3}$	$\frac{2}{3}$

TABLE I: Representations of VLQs and their quantum numbers under the SM gauge group.

These representations allow for couplings between VLQs and SM gauge bosons and quarks. The kinetic and mass terms of the VLQs are described as [61],

$$\mathcal{L} = \sum_F \bar{F}(i\not{D} - M_F)F \tag{1}$$

where $F = \{U, D, Q_1, Q_5, Q_7, T_1, T_2\}$, $D_\mu = \partial_\mu + ig_1 Y_F B_\mu + ig_2 S^I W^I_\mu + ig_s T^A G^A_\mu$, $\lambda^A (A = 1, 2, \cdots, 8)$ and $\tau^I (I = 1, 2, 3)$, related to the Gell-Mann and Pauli matrices via $T^A = \frac{1}{2}\lambda^A$ and $S^I = \frac{1}{2}\tau^I$, respectively. In our simplified model, we use an effective Lagrangian framework for the interactions of a VLQ Y with the SM quarks through W boson exchange, including as Y free parameters $\kappa_Y^{i,L/R}$ (couplings) and m_Y (mass) [63]:

$$\mathcal{L} = \left\{ \kappa_Y^{i,L/R} \sqrt{\frac{\zeta_i}{\Gamma_W^0}} \frac{g}{\sqrt{2}} \left[\bar{Y}_{L/R} W_\mu^- \gamma^\mu d^i_{L/R} \right] + \text{H.c.} \right\} + m_Y \bar{Y} Y, \tag{2}$$

where $d^i_{L/R} (i = 1, 2, 3)$ represent the three types of quarks in the SM while L and R stand for the left-handed and right-handed chiralities, respectively. We assume that the Y only

couples to the third generation quarks of the SM, that is, Y decays 100% into Wb and therefore $\zeta_1 = \zeta_2 = 0, \zeta_3 = 1$. Considering that the Y mass is much greater than any SM quark mass (m_q), that is, $m_Y \gg m_q$, the kinematic function can be approximated as $\Gamma^0_W = 1$ [63], so that the above Lagrangian can be simplified as

$$\mathcal{L} = \left\{ \frac{g\kappa_Y^{3,L/R}}{\sqrt{2}} \left[\bar{Y}_{L/R} W^-_\mu \gamma^\mu b_{L/R} \right] + \text{H.c.} \right\} + m_Y \bar{Y} Y, \tag{3}$$

where g is the EW coupling constant. Comparing the Lagrangian for the (B, Y) doublet and (T, B, Y) triplet, we observe that the relationship between the coupling $\kappa_Y^{3,L/R}$ and mixing angle $\theta^{L/R}$ is $\sin\theta^{L/R} = \kappa_Y^{3,L/R}$ for the doublet and $\sin\theta^{L/R} = \sqrt{2}\kappa_Y^{3,L/R}$ for the triplet, with details to be found in Appendix A. Taking into account the relationship $\tan\theta^L = \frac{m_b}{m_B}\tan\theta^R$ and $\tan\theta^R = \frac{m_b}{m_B}\tan\theta^L$ as well as the condition $m_B \gg m_b$, we can assume $\kappa_Y^{3,L} = 0$ for the doublet and $\kappa_Y^{3,R} = 0$ for the triplet. (In the subsequent content, we will use κ_Y to denote $\kappa_Y^{3,R}$ for the sake of simplicity.) The decay width of the VLQ Y can be expressed as [64],

$$\Gamma(Y \to Wq) = \frac{\alpha_e \kappa_Y^2}{16\sin^2\theta_W} \frac{(m_W^2 - m_Y^2)^2(2m_W^2 + m_Y^2)}{m_W^2 m_Y^3}, \tag{4}$$

where $\alpha_{\text{EM}} = \frac{g'^2}{4\pi}$, g' is the Electro-Magnetic (EM) coupling constant and θ_W the EW mixing angle. In this paper, we solely focus on the Narrow Width Approximation (NWA), which we use for the purpose of simplifying scattering amplitude calculations. However, it is worth noting that several studies [31, 40, 65, 66] have highlighted the limitations of the NWA in scenarios involving new physics with VLQs. Specifically, it becomes imperative to consider a finite width when this becomes larger than $\alpha_{\text{EM}} \approx 1\%$, given the substantial interference effects emerging between VLQ production and decay channels, coupled with their interactions with the corresponding irreducible backgrounds. To address the limitations of our approach then, we will also present the ratio Γ_Y/m_Y in our subsequent results and we emphasise since now that, crucially, for the region where $\Gamma_Y/m_Y > 1\%$, our sensitivities may be under- or over-estimated, as such interferences could be positive or negative, respectively. Also, before starting with our numerical analysis, we remind the reader that one can apply the results of our forthcoming simulations to a specific VLQ representation, such as, e.g., (B, Y) or (T, B, Y), by utilizing the aforementioned relationships.

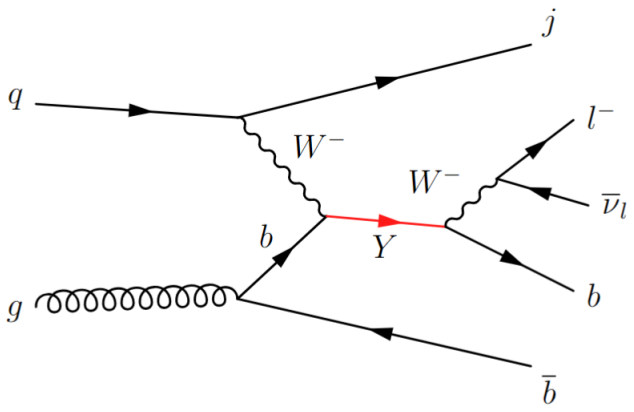

FIG. 1: Representative Feynman diagram of single Y (in red) production followed by its subsequent decay $Y \to W^-(\to l^-\bar{\nu}_l)b$. Here, q in the initial state represents one of the first two-generation quarks and bottom quark, j in the final state represents one of the first two-generation jets, b in the intermediate (final) state represents a b-quark (jet) while l^- represents either an electron or muon. Notice that, since we use the five flavor scheme, the $g \to b\bar{b}$ splitting in the diagram is actually accounted for through the PDF evolution.

In Figure 1, we show a representative Feynman diagram of the signal production $pp \to Y\bar{b}j$ and decay chain $Y \to W^-(\to l^-\bar{\nu}_l)b$. We expect the W boson and the high-momentum b-jet to exhibit a back-to-back alignment in the transverse plane, originating from the decay of the massive Y quark. The topology also encompasses an outgoing light quark, often resulting in a forward jet within the detector. Furthermore, the second b-jet arising from the splitting of a gluon into a pair of b-quarks can be observed in either the forward or central region. According to these features of signal events, the primary SM backgrounds include $pp \to t\bar{b}j$, $pp \to W^+W^-b$, $pp \to Zbj$, $pp \to W^+bj$, and their charge conjugated processes. Among them, $pp \to t\bar{b}j$ and $pp \to W^+W^-b$ are irreducible backgrounds, while the others are reducible backgrounds. We have also assessed additional backgrounds, such as $pp \to t\bar{t}$, and found that their contribution can be ignored based on the selection criteria that will be discussed later.

The signal production cross section is determined not only by the mass m_Y but also by the coupling strength κ_Y. The cross section is directly proportional to κ_Y^2 for a fixed m_Y as long as the NWA is met [66]. In Figure 2, we show the tree-level cross sections for

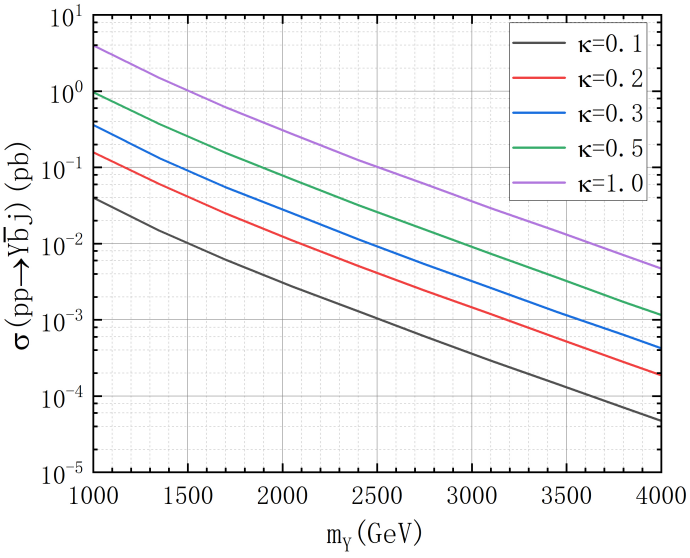

FIG. 2: The tree-level cross sections for single Y production as a function of the mass m_Y for various values of the coupling κ_Y. The charge conjugated process has also been taken into account.

single Y production as a function of the mass m_Y. We can see that, as m_Y increases, the cross section gradually decreases due to a smaller phase space.

In Figure 3, we show the tree-level cross sections for the signal benchmarks $m_Y = 1000$ GeV (labeled as Y_{1000}) and $m_Y = 1500$ GeV (labeled as Y_{1500}) with $\kappa_Y = 0.1$ and $\kappa_Y = 0.5$ as well as the tree-level cross sections for the background processes. It is evident that the rates for the latter are significantly larger than those for the former. Consequently, we should design efficient selection criteria (in terms of kinematic cuts) to reduce the number of background events while preserving the signal events. Furthermore, the cross sections for both signal and backgrounds increase with increasing collider energy.

The Next-to-Leading Order (NLO) (or even higher order) QCD corrections for the SM background cross sections at the LHC have been extensively explored in Refs. [67–71]. The K factors associated with the background cross sections adopted in our calculations are summarized in Table II. (Note that, despite they change somewhat with energy, we neglect here changes of K factors values at different colliders, like in Ref. [72].)

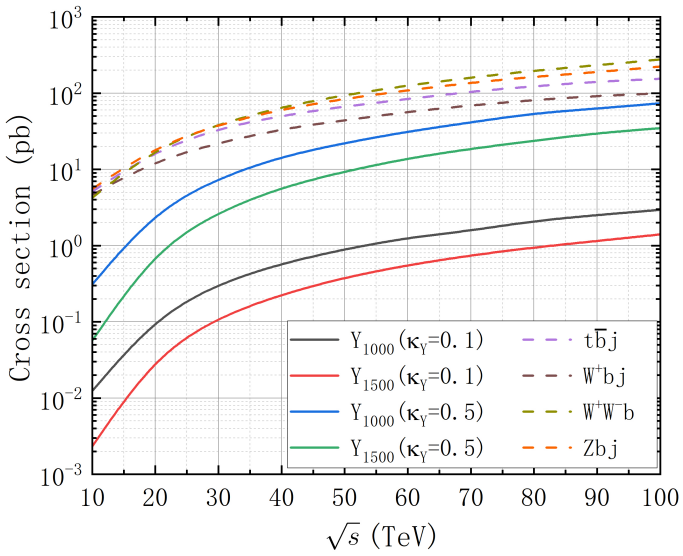

FIG. 3: The tree-level cross sections as a function of the center-of-mass energy $\sqrt{s}$ for the signal benchmarks and backgrounds. Solid lines represent the signal processes and dashed lines represent the background processes. The cross sections also include the corresponding charge conjugated processes.

Processes	Zbj	W^+bj	W^+W^-b	$t\bar{b}j$
K factor	1.3 [68]	1.9 [69]	2.1 [69]	1.4 [70, 71]

TABLE II: K factors representing the QCD corrections for the background processes.

There are stringent limits from the oblique parameters S, T and U in EWPOs [17, 61, 73–83]. These oblique parameters relate to the weak isospin current $J^\mu_{1,2,3}$ and the electromagnetic current $J^\mu_Q = J^\mu_3 + J^\mu_Y$, involving their vacuum-polarization amplitudes as defined in references [74, 76]:

$$\begin{aligned} S &\equiv -\frac{16\pi}{m_Z^2}\left\{\Sigma_{33}(m_Z^2) - \Sigma_{33}(0) - \Sigma_{3Q}(m_Z^2)\right\} \\ &= \frac{16\pi}{m_Z^2}\left\{\Sigma_{3Y}(m_Z^2) - \Sigma_{3Y}(0)\right\}, \end{aligned} \tag{5}$$

$$T \equiv \frac{4\pi}{\sin^2\theta_W \cos^2\theta_W m_Z^2}\left\{\Sigma_{33}(0) - \Sigma_{11}(0)\right\}, \tag{6}$$

$$U \equiv \frac{16\pi}{m_Z^2}\left\{\Sigma_{33}(m_Z^2) - \Sigma_{33}(0)\right\} - \frac{16\pi}{m_W^2}\left\{\Sigma_{11}(m_Z^2) - \Sigma_{11}(0)\right\}, \tag{7}$$

where m_W and m_Z denote the mass for W and Z boson, respectively. The Z-boson current, represented by $e(J_3^\mu - s_W^2 J_Q^\mu)/(\sin\theta_W \cos\theta_W)$, involves e linked to the fine-structure constant α through $e^2 \equiv 4\pi\alpha$. Consequently, the oblique parameters can be reformulated using the vacuum polarizations of the SM gauge bosons as:

$$\alpha T = \frac{\Sigma_{ZZ}^{\text{new}}(0)}{m_Z^2} - \frac{\Sigma_{WW}^{\text{new}}(0)}{m_W^2} \tag{8}$$

$$\begin{aligned}\frac{\alpha}{\sin^2 2\theta_W} S &= -\frac{\Sigma_{ZZ}^{\text{new}}(m_Z^2) - \Sigma_{ZZ}^{\text{new}}(0)}{m_Z^2} + \left.\frac{\partial\Sigma_{\gamma\gamma}^{\text{new}}(p^2)}{\partial p^2}\right|_{p^2=0} + \frac{\cos 2\theta_W}{\cos\theta_W \sin\theta_W}\left.\frac{\partial\Sigma_{\gamma Z}^{\text{new}}(p^2)}{\partial p^2}\right|_{p^2=0} \\ &\simeq -\left.\frac{\partial\Sigma_{ZZ}^{\text{new}}(p^2)}{\partial p^2}\right|_{p^2=0} + \left.\frac{\partial\Sigma_{\gamma\gamma}^{\text{new}}(p^2)}{\partial p^2}\right|_{p^2=0} + \frac{\cos 2\theta_W}{\cos\theta_W \sin\theta_W}\left.\frac{\partial\Sigma_{\gamma Z}^{\text{new}}(p^2)}{\partial p^2}\right|_{p^2=0}\end{aligned} \tag{9}$$

$$\begin{aligned}\frac{\alpha}{4\sin^2\theta_W} U &= -\frac{\Sigma_{WW}^{\text{new}}(m_W^2) - \Sigma_{WW}^{\text{new}}(0)}{m_W^2} + \cos^2\theta_W \frac{\Sigma_{ZZ}^{\text{new}}(m_Z^2) - \Sigma_{ZZ}^{\text{new}}(0)}{m_Z^2} \\ &\quad + \sin^2\theta_W \left.\frac{\partial\Sigma_{\gamma\gamma}^{\text{new}}(p^2)}{\partial p^2}\right|_{p^2=0} + \sin 2\theta_W \left.\frac{\partial\Sigma_{\gamma Z}^{\text{new}}(p^2)}{\partial p^2}\right|_{p^2=0} \\ &\simeq -\frac{\partial\Sigma_{WW}^{\text{new}}(p^2)}{\partial p^2}|_{p^2=0} + \cos^2\theta_W \frac{\partial\Sigma_{ZZ}^{\text{new}}(p^2)}{\partial p^2}|_{p^2=0} + \sin^2\theta_W \frac{\partial\Sigma_{\gamma\gamma}^{\text{new}}(p^2)}{\partial p^2}|_{p^2=0} \\ &\quad + \sin 2\theta_W \frac{\partial\Sigma_{\gamma Z}^{\text{new}}(p^2)}{\partial p^2}|_{p^2=0}.\end{aligned} \tag{10}$$

The contributions in the doublet (B, Y) model to these oblique parameters can be approximated as follows [61]:

$$S \simeq \frac{1}{2\pi}\left\{-\frac{2}{3}\kappa_Y^2 \ln\frac{\mathcal{M}^2}{m_b^2} + \frac{11}{3}\kappa_Y^2\right\}, U \simeq -\frac{\kappa_Y^2}{2\pi}, T \simeq \frac{3m_t^2}{8\pi\sin^2\theta_W m_W^2}\kappa_Y^4 \frac{2\mathcal{M}^2}{3m_t^2} \tag{11}$$

Here, $\mathcal{M}^2 = (m_Y^2 - m_b^2\kappa_Y^2)/(1-\kappa_Y^2)$ and $m_W = m_Z\cos\theta_W$. For the numerical calculation, the χ^2 function for the oblique parameter fit should be less than 8.02 for three degrees of freedom to compute the 2σ limits, respectively. $S = -0.02 \pm 0.1$, $T = 0.03 \pm 0.12$, $U = 0.01 \pm 0.11$; there exists a strong correlation of 92% between the S and T parameters, while the U parameter exhibits an anti-correlation of -80% (-93%) with S (T) [84]. Specific numerical values of the input parameters are detailed in Eq. 12.

III. SIGNAL TO BACKGROUND ANALYSIS

The signal model file is sourced from FeynRules [85] and parton-level events are generated using MadGraph5_aMC@NLO [86] with the NNPDF23LO1 [87] Parton Distribution Function (PDFs). Dynamic factorization and renormalization scales, set as default in

MadEvent [88], are utilized. Subsequently, fast detector simulations are conducted using Delphes 3.4.2 [89] with the built-in detector configurations of the LHC Run-III, HL-LHC, HE-LHC [90] and FCC-hh [91]. Jets are clustered by FastJet [92] employing the anti-kt algorithm [93] with a distance parameter of $\Delta R = 0.4$. Furthermore, MadAnalysis 5 [94] is used to analyze both signal and background events. Finally, the EasyScan_HEP package [95] is utilized to connect these programs and scan the VLQ parameter space.

The numerical values of the input SM parameters are taken as follows [84]:

$$\begin{aligned} &m_b = 4.18 \text{ GeV}, \quad m_t = 172.69 \text{ GeV}, \quad m_Z = 91.1876 \text{ GeV}, \\ &\sin^2\theta_W = 0.22339, \quad \alpha(m_Z) = \frac{1}{127.951}, \quad \alpha_s(m_Z) = 0.1179. \end{aligned} \tag{12}$$

Considering the general detection capabilities of detectors, the following basic cuts are chosen:

$$\begin{aligned} &\Delta R(x,y) > 0.4 \qquad (x, y = l, j, b), \\ &p_T^l > 25 \text{ GeV}, \qquad |\eta_l| < 2.5, \\ &p_T^j > 20 \text{ GeV}, \qquad |\eta_j| < 5.0, \\ &p_T^b > 25 \text{ GeV}, \qquad |\eta_b| < 2.5, \end{aligned}$$

where $\Delta R = \sqrt{\Delta\Phi^2 + \Delta\eta^2}$ denotes the separation in the rapidity(η)–azimuth(ϕ) plane.

To handle the relatively small event number of signal (s) and background (b) events, we will use the median significance $\mathcal{Z}$ to estimate the expected discovery and exclusion reaches [96, 97],

$$\mathcal{Z}_{excl} = \sqrt{2\left[s - b\ln\left(\frac{b+s+x}{2b}\right) - \frac{1}{\delta^2}\ln\left(\frac{b-s+x}{2b}\right)\right] - (b+s-x)\left(1+\frac{1}{\delta^2 b}\right)}, \tag{13}$$

$$\mathcal{Z}_{disc} = \sqrt{2\left[(s+b)\ln\left(\frac{(s+b)(1+\delta^2 b)}{b+(s+b)\delta^2 b}\right) - \frac{1}{\delta^2}\ln\left(1+\frac{\delta^2 s}{1+\delta^2 b}\right)\right]}, \tag{14}$$

$$x = \sqrt{(s+b)^2 - \frac{4\delta^2 s b^2}{1+\delta^2 b}}, \tag{15}$$

where δ is the uncertainty that inevitably appears in the measurement of the background. In the completely ideal case, that is δ=0, Eq. (13) and (14) can be simplified as follows, respectively:

$$\mathcal{Z}_{excl} = \sqrt{2\left[s - b\ln\left(1+\frac{s}{b}\right)\right]}, \tag{16}$$

and

$$\mathcal{Z}_{disc} = \sqrt{2\left[(s+b)\ln\left(1+\frac{s}{b}\right)-s\right]}. \tag{17}$$

A. LHC Run-III and HL-LHC

Firstly, we establish a trigger that emulates the LHC Run-III and HL-LHC detector response based on the count of final state particles detected in each event. Given the limited efficiency of the detector in identifying jets, we adopt a lenient approach towards the number of jets. Consequently, the final trigger criteria are defined as follows: $N_l = 1$, $N_j \geq 2$, $N_j \leq 4$ and $N_b \geq 2$.

Considering that the mass of Y is notably greater than that of its decay products, the latter exhibit distinct spatial characteristics in pseudorapidity η and spatial separation ΔR compared to backgrounds. These differences inform our selection criteria. Furthermore,

Cuts	Y_{1500} (fb)	Y_{1800} (fb)	$t\bar{b}j$ (fb)	W^+bj (fb)	W^+W^-b (fb)	Zbj (fb)
Basic Cuts	1.99	0.97	13855.00	15016.00	18967.00	13897.00
Trigger	0.29	0.13	2227.40	775.10	1251.50	312.80
Cut 1	0.25	0.12	40.09	11.95	39.12	2.63
Cut 2	0.23	0.11	7.46	4.07	8.07	0.63
Cut 3	0.16	0.08	4.51	3.02	4.93	0.39
Cut 4	0.08	0.05	0.08	1.35	1.18	0.15
Cut 5	0.08	0.04	0.08	1.00	0.89	0.13
Cut 6	0.04	0.03	0.01	0.02	0.05	0.00
Cut 7	0.03	0.02	0.01	0.00	0.03	0.00

TABLE III: Cut flows of the signal with $\kappa_Y = 0.1$ and backgrounds at the 14 TeV HL-LHC, where the conjugate processes $pp \to \bar{t}bj$, $W^-\bar{b}j$, $W^+W^-\bar{b}$, $Z\bar{b}j$ have been included.

since the mass range of Y is much heavier than the particles originating from background processes, we anticipate that the transverse momentum (referred to as $\vec{p}_T$ and its magnitude denoted as p_T) of decay products of the Y state will be substantially larger than those of the same particles from background processes. Besides, we will also consider variables such as $\not{E}_T$, $\not{H}_T$ and M_T to distinguish the signal from the background. Here,

$\not{E}_T$ represents the magnitude of the sum of the transverse momenta of all visible final state particles, $\not{H}_T$ is analogous to $\not{E}_T$ but only considers all visible hadronic momenta while the transverse mass M_T is defined as follows:

$$\begin{aligned} M_T^2 &\equiv [E_T(1) + E_T(2)]^2 - [\vec{p}_T(1) + \vec{p}_T(2)]^2 \\ &= m_1^2 + m_2^2 + 2[E_T(1)E_T(2) - \vec{p}_T(1) \cdot \vec{p}_T(2)], \end{aligned}$$

where $E_T(i) = \sqrt{p_T^2(i) + m_i^2}$ and $m_i^2 = p_i^2$ with p_i representing a 4-vector.

In Figure 4, we present the normalized distributions of $p_T^{j_1}$, $M_{b_1 l_1}$, $M_{j_1 j_2}$, $M_T^{b_2 l_1}$, $M_T^{b_1 l_1}$, $\Delta R_{j_1,b_1}$, $\not{H}_T$ and $\not{E}_T$ for both $m_Y = 1500$ GeV and $m_Y = 1800$ GeV with $\kappa_Y = 0.1$ as well as for the background processes. Based on these distributions, we have devised the following selection criteria to distinguish the signal from the various backgrounds[1]:

- Trigger: $N_l = 1$, $N_j \geq 2$, $N_j \leq 4$, and $N_b \geq 2$;
- Cut-1: $p_T^{j_1} > 300$ GeV;
- Cut-2: $M_{b_1 l_1} > 500$ GeV;
- Cut-3: $M_{j_1 j_2} > 500$ GeV;
- Cut-4: $M_T^{b_1 l_1} > 200$ GeV and $M_T^{b_2 l_1} > 200$ GeV;
- Cut-5: $\Delta R_{j_1,b_1} < 1.0$;
- Cut-6: $\not{H}_T > 600$ GeV;
- Cut-7: $\not{E}_T > 200$ GeV.

By applying these cuts, we can see that the signal efficiencies for $m_Y = 1500$ GeV and $m_Y = 1800$ GeV are 1.35% and 2.41%, respectively. The higher efficiency for the latter can be attributed to the larger transverse boost of the final state originating from an heavier Y. Meanwhile, the background processes are significantly suppressed. For reference, we provide the cut flows in Table III.

[1] The subscript on the particle symbol is arranged according to the magnitude of the particle transverse momentum: e.g., in the case of b-jets, $p_T^{b_1}$ is greater than $p_T^{b_2}$.

We present the exclusion capability ($\mathcal{Z}_{\rm excl} = 2$) and discovery potential ($\mathcal{Z}_{\rm disc} = 5$) for Y with two different integrated luminosities, 1000 fb^{-1} and 3000 fb^{-1}, at the HL-LHC, as shown in the top line of Figure 7. This analysis considers both the ideal scenario without systematic uncertainties and the case with a 10% systematic uncertainty. In the presence of 10% systematic uncertainty, the Y can be excluded in the correlated parameter space of $\kappa_Y \in [0.044, 0.5]$ and $m_Y \in [1000\ \text{GeV}, 3099\ \text{GeV}]$ with an integrated luminosity of $L = 300$ fb^{-1}, which corresponds to the maximum achievable integrated luminosity during LHC Run-III. If the integrated luminosity is raised to 3000 fb^{-1}, aligning with the maximum achievable at the HL-LHC, the excluded parameter zones extend to $\kappa_Y \in [0.027, 0.5]$ and $m_Y \in [1000\ \text{GeV}, 3653\ \text{GeV}]$. Furthermore, the discovery regions are $\kappa_Y \in [0.072, 0.5]$ ([0.047, 0.5]) and $m_Y \in [1000\ \text{GeV}, 2621\ \text{GeV}]$ ([1000 GeV, 3047 GeV]) with $L = 300$ fb^{-1} (3000 fb^{-1}).

B. 27 TeV HE-LHC

Cuts	Y_{1500} (fb)	Y_{1800} (fb)	$t\bar{b}j$ (fb)	W^+bj (fb)	W^+W^-b (fb)	Zbj (fb)
Basic Cuts	16.86	10.01	41398.00	38670.00	69303.00	69658.00
Trigger	1.78	0.10	6224.50	2149.10	4445.40	1700.70
Cut 1	1.50	0.91	86.07	29.51	133.60	10.73
Cut 2	1.36	0.85	18.30	11.14	29.52	2.37
Cut 3	0.95	0.62	12.83	9.05	19.27	1.53
Cut 4	0.35	0.27	0.17	2.94	3.10	0.35
Cut 5	0.33	0.25	0.17	2.01	2.36	0.28
Cut 6	0.12	0.16	0.00	0.04	0.37	0.00
Cut 7	0.09	0.12	0.00	0.04	0.14	0.00

TABLE IV: Cut flows of the signal with $\kappa_Y = 0.1$ and backgrounds at the 27 TeV HE-LHC.

This section delves into the prospective signal of Y at the future 27 TeV HE-LHC. In Figure 5, we exhibit the normalized distributions for both signal and background processes, forming the basis for our distinctive selection criteria:

- Trigger: $N_l = 1$, $N_j \geq 2$, $N_j \leq 4$, and $N_b \geq 2$;

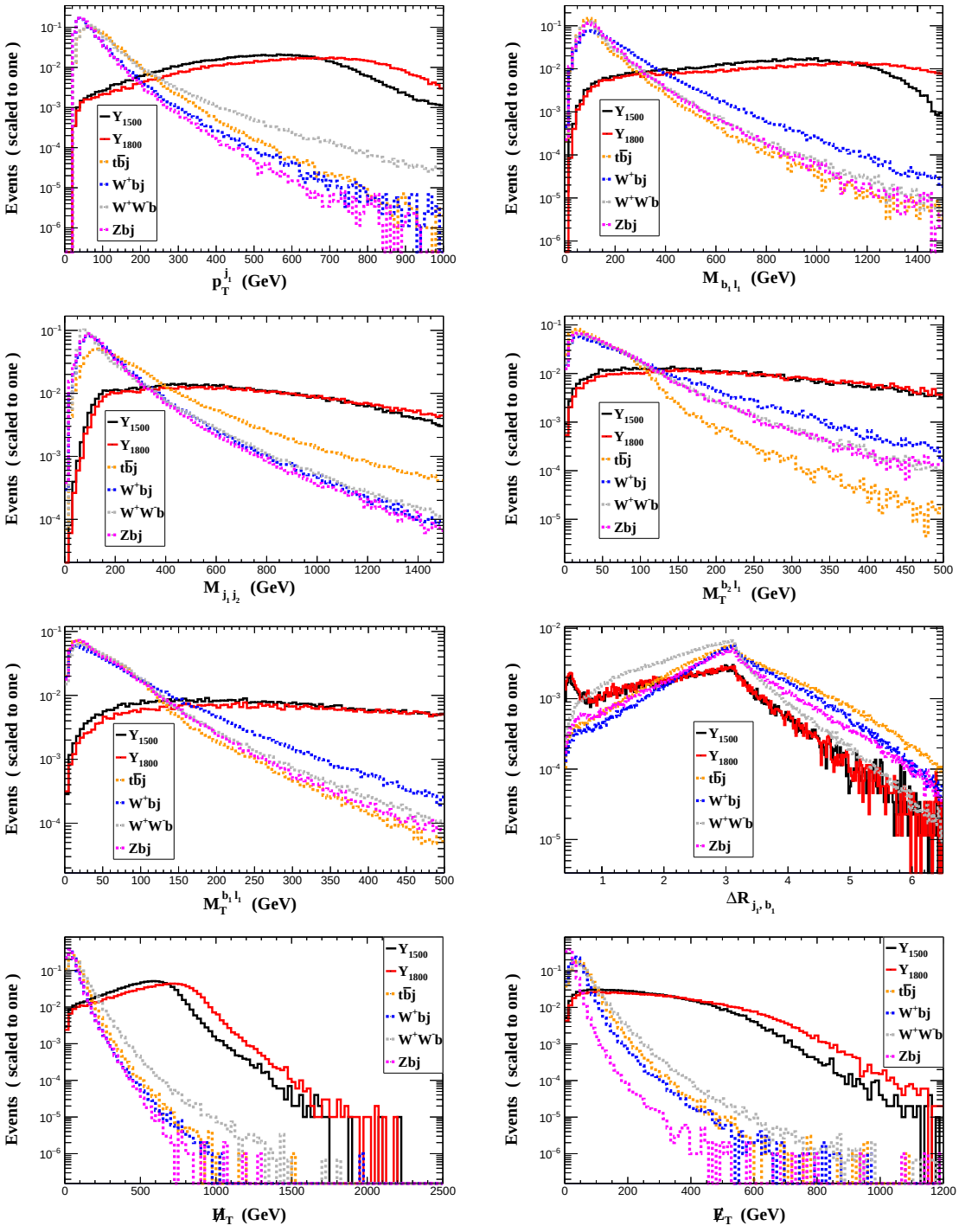

FIG. 4: Normalized distributions for the signals of $m_Y = 1500$ GeV and 1800 GeV and SM backgrounds at the HL-LHC. The conjugated processes have been included.

- Cut-1: $p_T^{j_1} > 350$ GeV;
- Cut-2: $M_{b_1 l_1} > 550$ GeV;

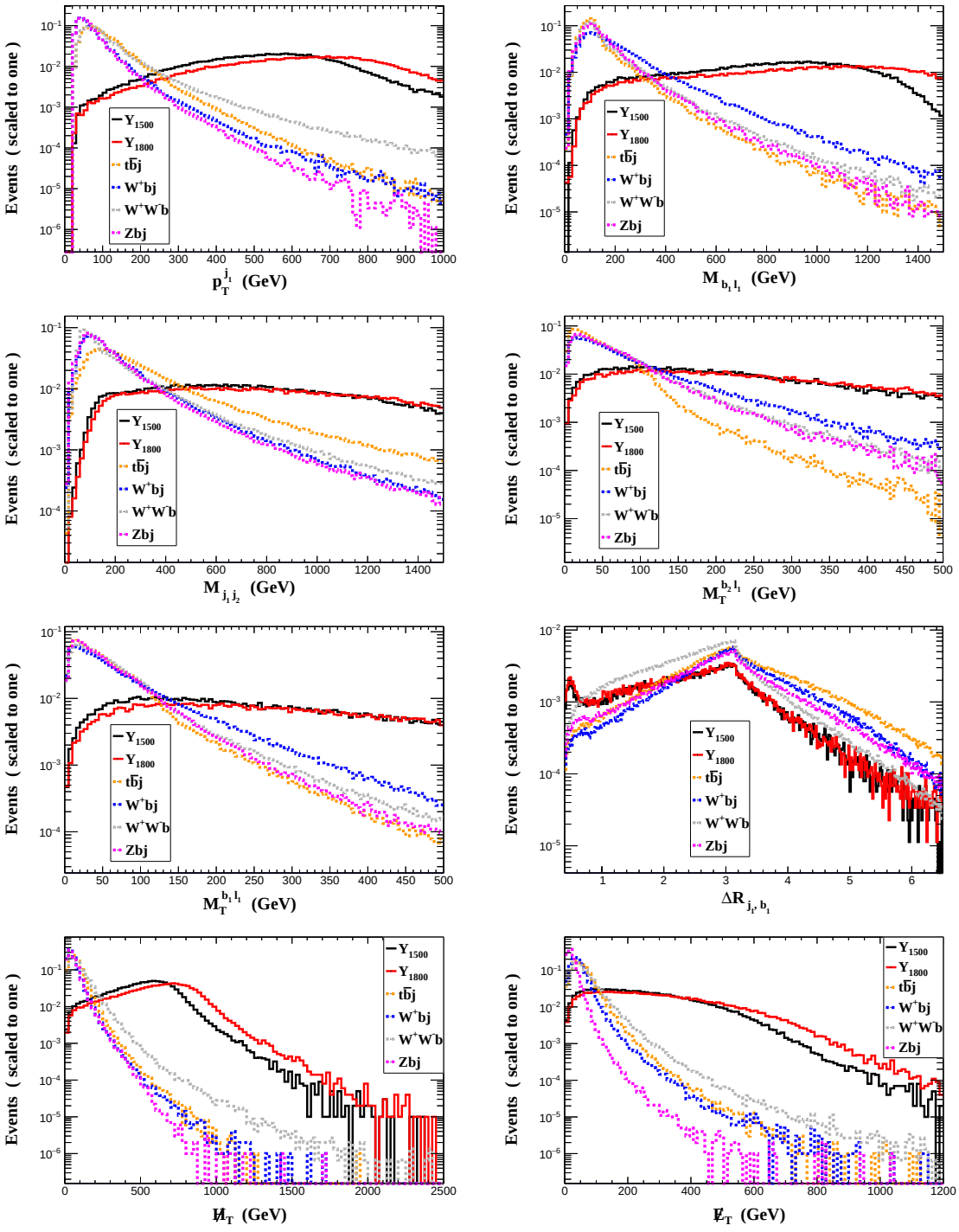

FIG. 5: Normalized distributions for the signals with $m_Y = 1500$ GeV and 1800 GeV and backgrounds at the HE-LHC.

- Cut-3: $M_{j_1 j_2} > 550$ GeV;
- Cut-4: $M_T^{b_2 l_1} > 250$ GeV and $M_T^{b_1 l_1} > 250$ GeV;

- Cut-5: $\Delta R_{j_1,b_1} < 0.5$;
- Cut-6: $\not{H}_T > 650$ GeV;
- Cut-7: $\not{E}_T > 200$ GeV.

The kinematic variables remain consistent with those of the 14 TeV case, but the cut threshold values for transverse momentum-based variables, such as $\not{H}_T > 650$ GeV, are higher than those in the 14 TeV case. This adjustment accounts for the increased center-of-mass energy. Detailed cut flows are outlined in Table IV and the exclusion capability and discovery potential are shown in the second row of Figure 7. The Y quark can be excluded within the correlated parameter space of $\kappa_Y \in [0.033, 0.5]$ and $m_Y \in [1000\text{ GeV}, 4783\text{ GeV}]$ with 10% systematic uncertainty for $L = 1000$ fb^{-1}. If the integrated luminosity is raised to the highest designed value 10 ab^{-1}, the excluded parameter regions can be extended to $\kappa_Y \in [0.029, 0.5]$ and $m_Y \in [1000\text{ GeV}, 4987\text{ GeV}]$. For $L = 3000$ fb^{-1}, the discovery regions are $\kappa_Y \in [0.053, 0.5]$ and $m_Y \in [1000\text{ GeV}, 3885\text{ GeV}]$. If the integrated luminosity is raised to the highest designed value 10 ab^{-1}, the discovery parameter regions can be extended to $\kappa_Y \in [0.051, 0.5]$ and $m_Y \in [1000\text{ GeV}, 3943\text{ GeV}]$.

C. 100 TeV FCC-hh

Cuts	Y_{1500} (fb)	Y_{1800} (fb)	$t\bar{b}j$ (fb)	W^+bj (fb)	W^+W^-b (fb)	Zbj (fb)
Basic Cuts	261.26	183.18	237538.00	206093.00	573258.00	291603.00
Trigger	13.44	8.42	33633.00	17209.00	40939.00	6363.90
Cut 1	6.37	4.20	209.30	112.70	605.90	18.95
Cut 2	5.63	3.89	54.16	48.43	163.30	7.58
Cut 3	3.30	2.51	3.33	23.91	53.74	3.21
Cut 4	3.14	2.43	3.33	17.72	45.12	3.21
Cut 5	1.40	1.70	0.48	1.65	6.15	0.00
Cut 6	0.81	1.16	0.24	0.21	2.87	0.00

TABLE V: Cut flows of the signal with $\kappa_Y = 0.1$ and backgrounds at the 100 TeV FCC-hh.

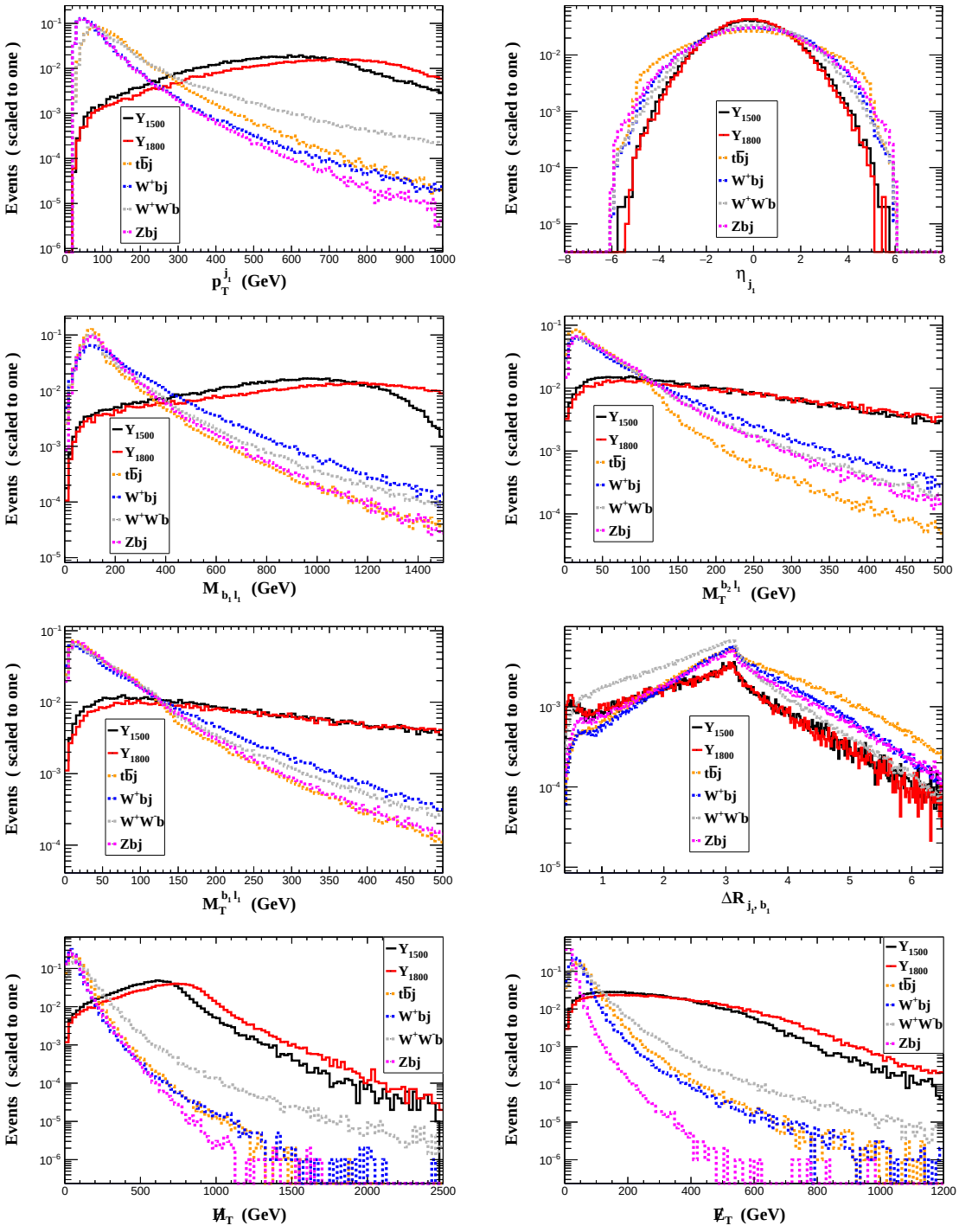

FIG. 6: Normalized distributions for the signals with $m_Y = 1500$ GeV and 1800 GeV, and backgrounds at the FCC-hh.

Here, we explore the anticipated signal of Y in the context of the future 100 TeV FCC-hh. The figures in Figure 6 portray normalized distributions for both signal and

background processes, laying the groundwork for our distinctive selection criteria:

- Trigger: $N_l = 1$, $N_j \geq 2$, $N_j \leq 4$, and $N_b \geq 2$;
- Cut-1: $p_T^{j_1} > 350$ GeV, $|\eta_{j_1}| < 1$;
- Cut-2: $M_{b_1,l_1} > 550$ GeV;
- Cut-3: $M_T^{b_2 l_1} > 150$ GeV and $M_T^{b_1 l_1} > 250$ GeV;
- Cut-4: $\Delta R_{j_1,b_1} < 0.5$ GeV;
- Cut-5: $\not{H}_T > 650$ GeV;
- Cut-6: $\not{E}_T > 300$ GeV.

Compared to previous cases, an additional variable, η_{j_1}, is introduced here. Upon analyzing the distributions of η_{j_1}, it is apparent that the signal tends to be more central than the backgrounds. Thus, we require $|\eta_{j_1}| < 1$. The signal efficiencies for $m_Y = 1500$ GeV and $m_Y = 1800$ GeV are 0.20% and 0.45%, respectively. Notably, there is a significant suppression in the background processes. Comprehensive cut flows are provided in Table V. The exclusion capability and discovery potential are illustrated in the final row of Figure 7. It is evident that systematic uncertainty has a considerable impact on the results. Even with a 10% systematic uncertainty, the parameter space region will significantly shrink. Accounting for the 10% systematic uncertainty, the Y quark can be excluded within the correlated parameter space of $\kappa_Y \in [0.051, 0.5]$ and $m_Y \in [1000\text{ GeV}, 6610\text{ GeV}]$ at the highest design value of luminosity, $L = 30$ ab^{-1}. Additionally, the Y state can be discovered within $\kappa_Y \in [0.088, 0.5]$ and $m_Y \in [1000\text{ GeV}, 4624\text{ GeV}]$ at $L = 30$ ab^{-1}.

IV. SUMMARY

In a simplified model, we have investigated the single production of a doublet VLQ denoted by Y in the Wb decay channel at the the $\sqrt{s} = 14$ TeV HL-LHC, $\sqrt{s} = 27$ TeV HE-LHC and $\sqrt{s} = 100$ TeV FCC-hh, following its production via $pp \to Ybj$, with the W decaying leptonically (into electrons and muons plus their respective neutrinos). We

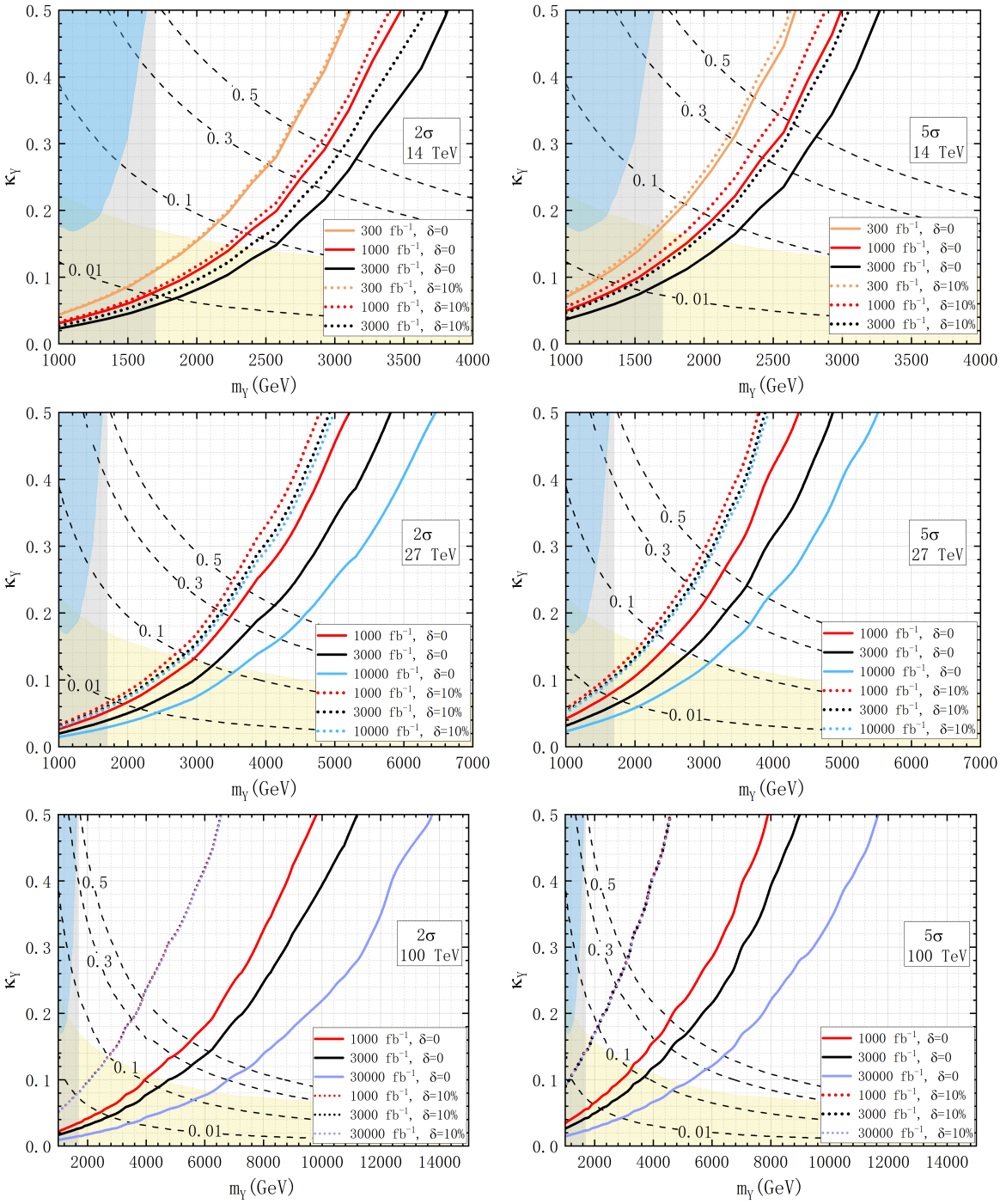

FIG. 7: The exclusion capability ($\mathcal{Z}_{\rm excl} = 2$) and discovery potential ($\mathcal{Z}_{\rm disc} = 5$) for the Y state at the LHC Run-III and HL-LHC, $\sqrt{s} = 27$ TeV HE-LHC and $\sqrt{s} = 100$ TeV FCC-hh. Solid lines represent the ideal scenario without systematic uncertainty, the dotted lines represent the scenario with a 10% systematic uncertainty. Dashed lines denote the contours of Γ_Y/m_Y. The blue (grey) shaded area indicates the exclusion region of the current LHC at $\sqrt{s} = 13$ TeV with L =36.1 fb^{-1} (140 fb^{-1}), as reported in Ref. [58] (Ref. [60]). Meanwhile, the yellow shaded area denotes the allowed region for the oblique parameters S, T and U, considering the current measurements in Ref. [84].

Colliders	L/fb^{-1}	Uncertainty	Exclusion		Discovery	
			κ_Y	m_Y(GeV)	κ_Y	m_Y(GeV)
LHC Run-III	300	0	[0.043,0.5]	[1000,3111]	[0.069,0.5]	[1000,2665]
	300	10%	[0.044,0.5]	[1000,3099]	[0.072,0.5]	[1000,2621]
14 TeV HL-LHC	1000	0	[0.031,0.5]	[1000,3486]	[0.049,0.5]	[1000,2988]
	3000	0	[0.023,0.5]	[1000,3820]	[0.037,0.5]	[1000,3267]
	1000	10%	[0.033,0.5]	[1000,3398]	[0.055,0.5]	[1000,2880]
	3000	10%	[0.027,0.5]	[1000,3653]	[0.047,0.5]	[1000,3047]
27 TeV HE-LHC	1000	0	[0.026,0.5]	[1000,5213]	[0.042,0.5]	[1000,4359]
	3000	0	[0.020,0.5]	[1000,5811]	[0.031,0.5]	[1000,4863]
	10000	0	[0.015,0.5]	[1000,6476]	[0.024,0.5]	[1000,5513]
	1000	10%	[0.033,0.5]	[1000,4783]	[0.057,0.5]	[1000,3783]
	3000	10%	[0.030,0.5]	[1000,4936]	[0.053,0.5]	[1000,3885]
	10000	10%	[0.029,0.5]	[1000,4987]	[0.051,0.5]	[1000,3943]
100 TeV FCC-hh	1000	0	[0.022,0.5]	[1000,9953]	[0.035,0.5]	[1000,7933]
	3000	0	[0.016,0.5]	[1000,11259]	[0.026,0.5]	[1000,9000]
	10000	0	[0.014,0.5]	[1000,12254]	[0.021,0.5]	[1000,10425]
	30000	0	[0.010,0.5]	[1000,13771]	[0.015,0.5]	[1000,11649]
	1000	10%	[0.051,0.5]	[1000,6610]	[0.088,0.5]	[1000,4624]
	3000	10%	[0.051,0.5]	[1000,6610]	[0.088,0.5]	[1000,4624]
	10000	10%	[0.051,0.5]	[1000,6610]	[0.088,0.5]	[1000,4624]
	30000	10%	[0.051,0.5]	[1000,6610]	[0.088,0.5]	[1000,4624]

TABLE VI: Summary for 2σ exclusion limits and 5σ signal discoveries at the LHC Run-III and HL-LHC, $\sqrt{s} = 27$ TeV HE-LHC and $\sqrt{s} = 100$ TeV FCC-hh.

have performed a detector level simulation for the signal and relevant SM backgrounds. Considering a systematic uncertainty of 10% with an integrated luminosity of 3000 fb^{-1}, the exclusion and discovery capabilities, as displayed in Table VI, can be described as follows: (1) The HL-LHC can exclude (discover) the correlated regions of $\kappa_Y \in [0.027, 0.5]$ ($[0.047, 0.5]$) and $m_Y \in [1000\text{ GeV}, 3653\text{ GeV}]$ ($[1000\text{ GeV}, 3047\text{ GeV}]$); (2) The HE-LHC

can exclude (discover) the correlated regions of $\kappa_Y \in [0.030, 0.5]$ ($[0.053, 0.5]$) and $m_Y \in [1000\ \text{GeV}, 4936\ \text{GeV}]$ ($[1000\ \text{GeV}, 3885\ \text{GeV}]$); (3) The FCC-hh can exclude (discover) the correlated regions of $\kappa_Y \in [0.051, 0.5]$ ($[0.088, 0.5]$) and $m_Y \in [1000\ \text{GeV}, 6610\ \text{GeV}]$ ($[1000\ \text{GeV}, 4624\ \text{GeV}]$).

Furthermore, we highlight that the stringent constraint on the VLQ Y, derived from the Y pair production search with $\text{BR}(Y \to W^- b) = 1$, imposes $m_Y > 1700$ GeV. In this context, we reassess the potential of LHC Run-III to explore the VLQ Y, revealing that the associated parameter regions of $\kappa_Y \in [0.044, 0.5]$ ($[0.072, 0.5]$) and $m_Y \in [1000\ \text{GeV}, 3099\ \text{GeV}]$ ($[1000\ \text{GeV}, 2621\ \text{GeV}]$) can be excluded (discovered) based on LHC Run-III luminosity. We foresee that our investigation will spur complementary explorations for a potential Y quark at forthcoming pp colliders.

Acknowledgements

This work of LS, YY and BY is supported by the Natural Science Foundation of Henan Province under Grant No. 232300421217, the National Research Project Cultivation Foundation of Henan Normal University under Grant No. 2021PL10, the China Scholarship Council under Grant No. 202208410277 and also powered by the High Performance Computing Center of Henan Normal University. The work of SM is supported in part through the NExT Institute, the Knut and Alice Wallenberg Foundation under the Grant No. KAW 2017.0100 (SHIFT) and the STFC Consolidated Grant No. ST/ L000296/1.

A. APPENDIX: RELATIONSHIP BETWEEN EQ. (1) AND EQ. (3)

In the appendix, we provide the relationship between the (B, Y) doublet representation and the simplified model used in the simulation. However, we do not present the relationship between the (X, B, Y) triplet representation and the simplified model here because it can be easily derived from the remainder of this Appendix.)

The Lagrangian for the Y coupling with the SM gauge fields and the Y mass term is

$$\mathcal{L} = \bar{Q}_5(i\not{D} - M_F)Q_5 \tag{A.1}$$

where one has

$$Q_5 = \begin{pmatrix} B_0 \\ Y_0 \end{pmatrix}, \bar{Q}_5 = (\bar{B}_0, \bar{Y}_0), \not{D} = \gamma^\mu D_\mu, D_\mu = \partial_\mu + ig'Y_F B_\mu + \frac{i}{2}g\tau^I W_\mu^I \tag{A.2}$$

and the weak isospin g and weak hypercharge g' are the $\mathrm{SU}(2)_L$ and $\mathrm{U}(1)_Y$ couplings, respectively. We use a subscript 0 to represent the interaction eigenstates. The unphysical fields B_μ and W_μ^I $(I = 1, 2, 3)$ can be transformed into the physical fields of the photon A_μ, the neutral Z boson Z_μ and charged W bosons $W_\mu^\pm$ via the following equations:

$$\begin{aligned} B_\mu &= \cos\theta_W A_\mu - \sin\theta_W Z_\mu, W_\mu^3 = \sin\theta_W A_\mu + \cos\theta_W Z_\mu, \\ W_\mu^1 &= \frac{1}{\sqrt{2}}(W_\mu^+ + W_\mu^-), W_\mu^2 = \frac{i}{\sqrt{2}}(W_\mu^+ - W_\mu^-) \end{aligned} \tag{A.3}$$

where θ_W is the Weinberg angle, which can be expressed via $\sin\theta_W = \frac{e}{g}$ and $\cos\theta_W = \frac{e}{g'}$. Here, M_F is a free mass parameter. Considering the charge of Y, the Lagrangian for the Y coupling with the SM gauge fields is

$$\begin{aligned} \mathcal{L}_{Q_5Q_5V} &= \bar{Q}_5 \left(\frac{5}{6}g'B_\mu - \frac{g}{2} \begin{bmatrix} W_\mu^3 & W_\mu^1 - iW_\mu^2 \\ W_\mu^1 + iW_\mu^2 & -W_\mu^3 \end{bmatrix} \right) \gamma^\mu Q_5 \\ &= \bar{Q}_5 \begin{bmatrix} \frac{1}{3}eA_\mu - \frac{g}{2\cos\theta}\left(1 + \frac{2}{3}\sin^2\theta\right) Z_\mu & -\frac{g}{\sqrt{2}}W_\mu^+ \\ -\frac{g}{\sqrt{2}}W_\mu^- & \frac{4}{3}eA_\mu + \frac{g}{2\cos\theta}\left(1 - \frac{8}{3}\sin^2\theta\right) Z_\mu \end{bmatrix} \gamma^\mu Q_5 \\ &= \frac{1}{3}e\bar{B}_0 A_\mu \gamma^\mu B_0 - \frac{g}{2\cos\theta}\left(1 + \frac{2}{3}\sin^2\theta\right) \bar{B}_0 Z_\mu \gamma^\mu B_0 \\ &\quad + \frac{4}{3}e\bar{Y}_0 A_\mu \gamma^\mu Y_0 + \frac{g}{2\cos\theta}\left(1 - \frac{8}{3}\sin^2\theta\right) \bar{Y}_0 Z_\mu \gamma^\mu Y_0 \\ &\quad - \frac{g}{\sqrt{2}}\bar{Y}_0 W_\mu^- \gamma^\mu B_0 - \frac{g}{\sqrt{2}}\bar{B}_0 W_\mu^+ \gamma^\mu Y_0. \end{aligned} \tag{A.4}$$

In our study, (B, Y) states exclusively couple with the third-generation quarks of the SM. Therefore, the Lagrangian for the mass term of the bottom quark mass eigenstate b and its partner mass eigenstate B can be written as

$$\mathcal{L}_{\text{mass}} = -\begin{pmatrix} \bar{b}_0^L & \bar{B}_0^L \end{pmatrix} \begin{pmatrix} y_{33}^d \frac{v}{\sqrt{2}} & y_{34}^d \frac{v}{\sqrt{2}} \\ y_{43}^d \frac{v}{\sqrt{2}} & M^0 \end{pmatrix} \begin{pmatrix} b_0^R \\ B_0^R \end{pmatrix} + \text{H.c.} \tag{A.5}$$

where $v = 246$ GeV is the Vacuum Expectation Value (VEV) of the Higgs field, M^0 is a bare mass term, y_{33}^d and y_{43}^d are Yukawa coupling coefficients while $y_{34}^d = 0$ for doublets. The mass matrix can be diagonalized by the two mixing matrices V^L and V^R, as follows:

$$\begin{pmatrix} b_0^{L,R} \\ B_0^{L,R} \end{pmatrix} = V^{L,R} \begin{pmatrix} b^{L,R} \\ B^{L,R} \end{pmatrix} \tag{A.6}$$

where L and R stands for the left-hand and right-hand chiralities, respectively. There exists the following relationship too: $B_0 = B_0^L + B_0^R$ and $Y_0 = Y_0^L + Y_0^R$. The 2×2 unitary matrices V^L and V^R can be parameterized by the mixing angles θ^L and θ^R, respectively, as

$$V^{L,R} = \begin{pmatrix} \cos\theta^{L,R} & \sin\theta^{L,R} \\ -\sin\theta^{L,R} & \cos\theta^{L,R} \end{pmatrix} \tag{A.7}$$

We can then determine the expressions $B_0^{L,R} = -\sin\theta^{L,R} b^{L,R} + \cos\theta^{L,R} B^{L,R}$. For Y, it is as simple as $Y_0^{L,R} = Y^{L,R}$, where Y represents the mass eigenstate. This is because there are no $\pm 4/3$ particles in the SM. Therefore, we can derive the interactions between the Y, W and b states as follows:

$$\begin{aligned} \mathcal{L}_{YW^{\pm}b} &= -\frac{g}{\sqrt{2}} \left(\bar{Y}^L + \bar{Y}^R\right) W_\mu^- \gamma^\mu \left(-\sin\theta^L b^L - \sin\theta^R b^R\right) + \text{H.c.} \\ &= \frac{g}{\sqrt{2}} \sin\theta^L \bar{Y}^L W_\mu^- \gamma^\mu b^L + \frac{g}{\sqrt{2}} \sin\theta^R \bar{Y}^R W_\mu^- \gamma^\mu b^R + \text{H.c.} \end{aligned} \tag{A.8}$$

Using unitary matrices, we can finally obtain

$$V^L \begin{pmatrix} y_{33}^d \frac{v}{\sqrt{2}} & y_{34}^d \frac{v}{\sqrt{2}} \\ y_{43}^d \frac{v}{\sqrt{2}} & M^0 \end{pmatrix} (V^R)^\dagger = \begin{pmatrix} m_b & 0 \\ 0 & m_B \end{pmatrix} \tag{A.9}$$

After performing calculations involving trigonometric function identities, we can obtain[2]:

$$\tan\theta^L = \frac{m_b}{m_B} \tan\theta^R \tag{A.10}$$

[2] For the (T, B, Y) triplet, $y_{43}^d = 0$, we can deduce instead that $\tan\theta^R = \frac{m_b}{m_B} \tan\theta^L$.

Since $m_B \gg m_b$, we can conclude that $\sin\theta^L \gg \sin\theta^R$ in the (B, Y) doublet. Therefore, our study primarily concentrates on the right-handed coupling part of the interactions involving the Y, W and b states.

[1] **ATLAS** Collaboration, G. Aad *et al.*, "Observation of a new particle in the search for the Standard Model Higgs boson with the ATLAS detector at the LHC," *Phys. Lett. B* **716** (2012) 1–29, arXiv:1207.7214 [hep-ex]. 2

[2] **CMS** Collaboration, S. Chatrchyan *et al.*, "Observation of a New Boson at a Mass of 125 GeV with the CMS Experiment at the LHC," *Phys. Lett. B* **716** (2012) 30–61, arXiv:1207.7235 [hep-ex]. 2

[3] N. Arkani-Hamed, A. G. Cohen, E. Katz, and A. E. Nelson, "The Littlest Higgs," *JHEP* **07** (2002) 034, arXiv:hep-ph/0206021. 2

[4] T. Han, H. E. Logan, B. McElrath, and L.-T. Wang, "Phenomenology of the little Higgs model," *Phys. Rev. D* **67** (2003) 095004, arXiv:hep-ph/0301040.

[5] S. Chang and H.-J. He, "Unitarity of little Higgs models signals new physics of UV completion," *Phys. Lett. B* **586** (2004) 95–105, arXiv:hep-ph/0311177.

[6] Q.-H. Cao and C.-R. Chen, "Signatures of extra gauge bosons in the littlest Higgs model with T-parity at future colliders," *Phys. Rev. D* **76** (2007) 075007, arXiv:0707.0877 [hep-ph]. 2

[7] K. Agashe, G. Perez, and A. Soni, "Collider Signals of Top Quark Flavor Violation from a Warped Extra Dimension," *Phys. Rev. D* **75** (2007) 015002, arXiv:hep-ph/0606293. 2

[8] K. Agashe, R. Contino, and A. Pomarol, "The Minimal composite Higgs model," *Nucl. Phys. B* **719** (2005) 165–187, arXiv:hep-ph/0412089. 2

[9] B. Bellazzini, C. Csáki, and J. Serra, "Composite Higgses," *Eur. Phys. J. C* **74** no. 5, (2014) 2766, arXiv:1401.2457 [hep-ph].

[10] M. Low, A. Tesi, and L.-T. Wang, "Twin Higgs mechanism and a composite Higgs boson," *Phys. Rev. D* **91** (2015) 095012, arXiv:1501.07890 [hep-ph].

[11] L. Bian, D. Liu, and J. Shu, "Low scale composite Higgs model and 1.8 $\sim$2 TeV diboson excess," *Int. J. Mod. Phys. A* **33** no. 11, (2018) 1841007, arXiv:1507.06018 [hep-ph].

[12] H.-J. He, C. T. Hill, and T. M. P. Tait, "Top Quark Seesaw, Vacuum Structure and Electroweak Precision Constraints," *Phys. Rev. D* **65** (2002) 055006, arXiv:hep-ph/0108041.

[13] H.-J. He, T. M. P. Tait, and C. P. Yuan, "New top flavor models with seesaw mechanism," *Phys. Rev. D* **62** (2000) 011702, arXiv:hep-ph/9911266. 2

[14] H.-J. He, T. M. P. Tait, and C. P. Yuan, "New top flavor models with seesaw mechanism," *Phys. Rev. D* **62** (2000) 011702, arXiv:hep-ph/9911266. 2

[15] X.-F. Wang, C. Du, and H.-J. He, "LHC Higgs Signatures from Topflavor Seesaw Mechanism," *Phys. Lett. B* **723** (2013) 314–323, arXiv:1304.2257 [hep-ph].

[16] H.-J. He, C. T. Hill, and T. M. P. Tait, "Top Quark Seesaw, Vacuum Structure and Electroweak Precision Constraints," *Phys. Rev. D* **65** (2002) 055006, arXiv:hep-ph/0108041. 2

[17] J. A. Aguilar-Saavedra, R. Benbrik, S. Heinemeyer, and M. Pérez-Victoria, "Handbook of vectorlike quarks: Mixing and single production," *Phys. Rev. D* **88** no. 9, (2013) 094010, arXiv:1306.0572 [hep-ph]. 2, 3, 8

[18] A. Banerjee, V. Ellajosyula, and L. Panizzi, "Heavy vector-like quarks decaying to exotic scalars: a case study with triplets," arXiv:2311.17877 [hep-ph]. 2

[19] R. Benbrik, M. Berrouj, M. Boukidi, A. Habjia, E. Ghourmin, and L. Rahili, "Search for single production of vector-like top partner T → H+b and H±→tb¯ at the LHC Run-III," *Phys. Lett. B* **843** (2023) 138024.

[20] B. Yang, S. Wang, X. Sima, and L. Shang, "Singlet vector-like T quark production in association with Wb at the CLIC," *Commun. Theor. Phys.* **75** no. 3, (2023) 035202. 2

[21] Q.-G. Zeng, Y.-S. Pan, and J. Zhang, "Search for the signal of vector-like bottom quark at LHeC in the final state with 3 b-jets," *Nucl. Phys. B* **995** (2023) 116347.

[22] A. C. Canbay and O. Cakir, "Investigating the single production of vectorlike quarks decaying into a top quark and W boson through hadronic channels at the HL-LHC," *Phys. Rev. D* **108** no. 9, (2023) 095006, arXiv:2307.12883 [hep-ph].

[23] A. Belyaev, R. S. Chivukula, B. Fuks, E. H. Simmons, and X. Wang, "Vectorlike top quark production via an electroweak dipole moment at a muon collider," *Phys. Rev. D* **108** no. 3, (2023) 035016, arXiv:2306.11097 [hep-ph].

[24] L. Shang and K. Sun, "Single vector-like quark X production in the tW channel at high energy pp colliders," *Nucl. Phys. B* **990** (2023) 116185.

[25] L. Shang, C. Chen, S. Wang, and B. Yang, "Single production of vector-like B quark

decaying into bZ at future ep colliders," *Nucl. Phys. B* **984** (2022) 115977.

[26] F. F. Freitas, J. a. Gonçalves, A. P. Morais, and R. Pasechnik, "Phenomenology at the large hadron collider with deep learning: the case of vector-like quarks decaying to light jets," *Eur. Phys. J. C* **82** no. 9, (2022) 826, arXiv:2204.12542 [hep-ph].

[27] R. Benbrik, M. Boukidi, and S. Moretti, "Probing Light Charged Higgs Bosons in the 2-Higgs Doublet Model Type-II with Vector-Like Quarks," arXiv:2211.07259 [hep-ph].

[28] G. Corcella, A. Costantini, M. Ghezzi, L. Panizzi, G. M. Pruna, and J. Šalko, "Vector-like quarks decaying into singly and doubly charged bosons at LHC," *JHEP* **10** (2021) 108, arXiv:2107.07426 [hep-ph].

[29] G. Corcella, A. Costantini, M. Ghezzi, L. Panizzi, G. M. Pruna, and J. Šalko, "Vector-like quarks decaying into singly and doubly charged bosons at LHC," *JHEP* **10** (2021) 108, arXiv:2107.07426 [hep-ph].

[30] A. Belyaev, R. S. Chivukula, B. Fuks, E. H. Simmons, and X. Wang, "Vectorlike top quark production via a chromomagnetic moment at the LHC," *Phys. Rev. D* **104** no. 9, (2021) 095024, arXiv:2107.12402 [hep-ph].

[31] A. Deandrea, T. Flacke, B. Fuks, L. Panizzi, and H.-S. Shao, "Single production of vector-like quarks: the effects of large width, interference and NLO corrections," *JHEP* **08** (2021) 107, arXiv:2105.08745 [hep-ph]. [Erratum: JHEP 11, 028 (2022)]. 5

[32] S. Dasgupta, R. Pramanick, and T. S. Ray, "Broad toplike vector quarks at LHC and HL-LHC," *Phys. Rev. D* **105** no. 3, (2022) 035032, arXiv:2112.03742 [hep-ph].

[33] S. J. D. King, S. F. King, S. Moretti, and S. J. Rowley, "Discovering the origin of Yukawa couplings at the LHC with a singlet Higgs and vector-like quarks," *JHEP* **21** (2020) 144, arXiv:2102.06091 [hep-ph].

[34] Y.-B. Liu and S. Moretti, "Search for single production of a top quark partner via the $T \to th$ and $h \to WW^*$ channels at the LHC," *Phys. Rev. D* **100** no. 1, (2019) 015025, arXiv:1902.03022 [hep-ph].

[35] R. Benbrik *et al.*, "Signatures of vector-like top partners decaying into new neutral scalar or pseudoscalar bosons," *JHEP* **05** (2020) 028, arXiv:1907.05929 [hep-ph].

[36] K.-P. Xie, G. Cacciapaglia, and T. Flacke, "Exotic decays of top partners with charge 5/3: bounds and opportunities," *JHEP* **10** (2019) 134, arXiv:1907.05894 [hep-ph].

[37] N. Bizot, G. Cacciapaglia, and T. Flacke, "Common exotic decays of top partners," *JHEP* **06** (2018) 065, arXiv:1803.00021 [hep-ph].

[38] G. Cacciapaglia, A. Carvalho, A. Deandrea, T. Flacke, B. Fuks, D. Majumder, L. Panizzi, and H.-S. Shao, "Next-to-leading-order predictions for single vector-like quark production at the LHC," *Phys. Lett. B* **793** (2019) 206–211, arXiv:1811.05055 [hep-ph].

[39] G. Cacciapaglia, A. Deandrea, N. Gaur, D. Harada, Y. Okada, and L. Panizzi, "The LHC potential of Vector-like quark doublets," *JHEP* **11** (2018) 055, arXiv:1806.01024 [hep-ph].

[40] A. Carvalho, S. Moretti, D. O'Brien, L. Panizzi, and H. Prager, "Single production of vectorlike quarks with large width at the Large Hadron Collider," *Phys. Rev. D* **98** no. 1, (2018) 015029, arXiv:1805.06402 [hep-ph]. 5

[41] **CMS** Collaboration, A. M. Sirunyan *et al.*, "Search for single production of vector-like quarks decaying to a b quark and a Higgs boson," *JHEP* **06** (2018) 031, arXiv:1802.01486 [hep-ex].

[42] D. Barducci and L. Panizzi, "Vector-like quarks coupling discrimination at the LHC and future hadron colliders," *JHEP* **12** (2017) 057, arXiv:1710.02325 [hep-ph].

[43] **CMS** Collaboration, A. M. Sirunyan *et al.*, "Search for single production of a vector-like T quark decaying to a Z boson and a top quark in proton-proton collisions at $\sqrt{s} = 13$ TeV," *Phys. Lett. B* **781** (2018) 574–600, arXiv:1708.01062 [hep-ex].

[44] C.-H. Chen and T. Nomura, "Single production of $X_{\pm 5/3}$ and $Y_{\mp 4/3}$ vectorlike quarks at the LHC," *Phys. Rev. D* **94** no. 3, (2016) 035001, arXiv:1603.05837 [hep-ph].

[45] A. Arhrib, R. Benbrik, S. J. D. King, B. Manaut, S. Moretti, and C. S. Un, "Phenomenology of 2HDM with vectorlike quarks," *Phys. Rev. D* **97** (2018) 095015, arXiv:1607.08517 [hep-ph].

[46] G. Cacciapaglia, A. Deandrea, N. Gaur, D. Harada, Y. Okada, and L. Panizzi, "Interplay of vector-like top partner multiplets in a realistic mixing set-up," *JHEP* **09** (2015) 012, arXiv:1502.00370 [hep-ph].

[47] A. Angelescu, A. Djouadi, and G. Moreau, "Vector-like top/bottom quark partners and Higgs physics at the LHC," *Eur. Phys. J. C* **76** no. 2, (2016) 99, arXiv:1510.07527 [hep-ph].

[48] L. Panizzi, "Vector-like quarks: t' and partners," *Nuovo Cim. C* **037** no. 02, (2014) 69–79.

[49] L. Panizzi, "Model-independent Analysis of Scenarios with Vector-like Quarks," *Acta Phys. Polon. Supp.* **7** no. 3, (2014) 631.

[50] G. Cacciapaglia, A. Deandrea, L. Panizzi, S. Perries, and V. Sordini, "Heavy Vector-like quark with charge 5/3 at the LHC," *JHEP* **03** (2013) 004, arXiv:1211.4034 [hep-ph].

[51] Y. Okada and L. Panizzi, "LHC signatures of vector-like quarks," *Adv. High Energy Phys.* **2013** (2013) 364936, arXiv:1207.5607 [hep-ph].

[52] G. Cacciapaglia, A. Deandrea, L. Panizzi, N. Gaur, D. Harada, and Y. Okada, "Heavy Vector-like Top Partners at the LHC and flavour constraints," *JHEP* **03** (2012) 070, arXiv:1108.6329 [hep-ph].

[53] F. del Aguila, L. Ametller, G. L. Kane, and J. Vidal, "Vector Like Fermion and Standard Higgs Production at Hadron Colliders," *Nucl. Phys. B* **334** (1990) 1–23. 2

[54] F. Gianotti *et al.*, "Physics potential and experimental challenges of the LHC luminosity upgrade," *Eur. Phys. J. C* **39** (2005) 293–333, arXiv:hep-ph/0204087. 2

[55] "High-Luminosity Large Hadron Collider (HL-LHC): Technical Design Report V. 0.1,". 2

[56] **FCC** Collaboration, A. Abada *et al.*, "HE-LHC: The High-Energy Large Hadron Collider: Future Circular Collider Conceptual Design Report Volume 4," *Eur. Phys. J. ST* **228** no. 5, (2019) 1109–1382. 2

[57] **FCC** Collaboration, A. Abada *et al.*, "FCC-hh: The Hadron Collider: Future Circular Collider Conceptual Design Report Volume 3," *Eur. Phys. J. ST* **228** no. 4, (2019) 755–1107. 2

[58] **ATLAS** Collaboration, M. Aaboud *et al.*, "Search for single production of vector-like quarks decaying into Wb in pp collisions at $\sqrt{s} = 13$ TeV with the ATLAS detector," *JHEP* **05** (2019) 164, arXiv:1812.07343 [hep-ex]. 2, 19

[59] **CMS** Collaboration, A. M. Sirunyan *et al.*, "Search for single production of vector-like quarks decaying into a b quark and a W boson in proton-proton collisions at $\sqrt{s} = 13$ TeV," *Phys. Lett. B* **772** (2017) 634–656, arXiv:1701.08328 [hep-ex]. 3

[60] **ATLAS** Collaboration, "Search for pair-production of vector-like quarks in lepton+jets final states containing at least one b-jet using the Run 2 data from the ATLAS experiment,". 3, 19

[61] J. Cao, L. Meng, L. Shang, S. Wang, and B. Yang, "Interpreting the W-mass anomaly in vectorlike quark models," *Phys. Rev. D* **106** no. 5, (2022) 055042, arXiv:2204.09477 [hep-ph]. 3, 4, 8, 9

[62] **CDF** Collaboration, T. Aaltonen *et al.*, "High-precision measurement of the W boson mass with the CDF II detector," *Science* **376** no. 6589, (2022) 170–176. 3

[63] M. Buchkremer, G. Cacciapaglia, A. Deandrea, and L. Panizzi, "Model Independent Framework for Searches of Top Partners," *Nucl. Phys. B* **876** (2013) 376–417, arXiv:1305.4172 [hep-ph]. 4, 5

[64] V. Cetinkaya, A. Ozansoy, V. Ari, O. M. Ozsimsek, and O. Cakir, "Single production of vectorlike Y quarks at the HL-LHC," *Nucl. Phys. B* **973** (2021) 115580, arXiv:2012.15308 [hep-ph]. 5

[65] D. Berdine, N. Kauer, and D. Rainwater, "Breakdown of the Narrow Width Approximation for New Physics," *Phys. Rev. Lett.* **99** (2007) 111601, arXiv:hep-ph/0703058. 5

[66] S. Moretti, D. O'Brien, L. Panizzi, and H. Prager, "Production of extra quarks at the Large Hadron Collider beyond the Narrow Width Approximation," *Phys. Rev. D* **96** no. 7, (2017) 075035, arXiv:1603.09237 [hep-ph]. 5, 6

[67] M. Czakon and A. Mitov, "NNLO corrections to top-pair production at hadron colliders: the all-fermionic scattering channels," *JHEP* **12** (2012) 054, arXiv:1207.0236 [hep-ph]. 7

[68] J. M. Campbell, R. K. Ellis, F. Maltoni, and S. Willenbrock, "Production of a Z boson and two jets with one heavy-quark tag," *Phys. Rev. D* **73** (2006) 054007, arXiv:hep-ph/0510362. [Erratum: Phys.Rev.D 77, 019903 (2008)]. 8

[69] J. M. Campbell, R. K. Ellis, F. Maltoni, and S. Willenbrock, "Production of a W boson and two jets with one b^- quark tag," *Phys. Rev. D* **75** (2007) 054015, arXiv:hep-ph/0611348. 8

[70] N. Kidonakis, "Single-top production in the Standard Model and beyond," in *13th Conference on the Intersections of Particle and Nuclear Physics*. 8, 2018. arXiv:1808.02934 [hep-ph]. 8

[71] E. Boos and L. Dudko, "The Single Top Quark Physics," *Int. J. Mod. Phys. A* **27** (2012)

1230026, arXiv:1211.7146 [hep-ph]. 7, 8

[72] B. Yang, X. Sima, S. Wang, and L. Shang, "Single vectorlike top quark production in the tZ channel at high energy pp colliders," *Phys. Rev. D* **105** no. 9, (2022) 096010. 7

[73] W. F. L. Hollik, "Radiative Corrections in the Standard Model and their Role for Precision Tests of the Electroweak Theory," *Fortsch. Phys.* **38** (1990) 165–260. 8

[74] M. E. Peskin and T. Takeuchi, "A New constraint on a strongly interacting Higgs sector," *Phys. Rev. Lett.* **65** (1990) 964–967. 8

[75] B. Grinstein and M. B. Wise, "Operator analysis for precision electroweak physics," *Phys. Lett. B* **265** (1991) 326–334.

[76] M. E. Peskin and T. Takeuchi, "Estimation of oblique electroweak corrections," *Phys. Rev. D* **46** (1992) 381–409. 8

[77] L. Lavoura and J. P. Silva, "The Oblique corrections from vector - like singlet and doublet quarks," *Phys. Rev. D* **47** (1993) 2046–2057.

[78] C. P. Burgess, S. Godfrey, H. Konig, D. London, and I. Maksymyk, "A Global fit to extended oblique parameters," *Phys. Lett. B* **326** (1994) 276–281, arXiv:hep-ph/9307337.

[79] I. Maksymyk, C. P. Burgess, and D. London, "Beyond S, T and U," *Phys. Rev. D* **50** (1994) 529–535, arXiv:hep-ph/9306267.

[80] G. Cynolter and E. Lendvai, "Electroweak Precision Constraints on Vector-like Fermions," *Eur. Phys. J. C* **58** (2008) 463–469, arXiv:0804.4080 [hep-ph].

[81] C.-Y. Chen, S. Dawson, and E. Furlan, "Vectorlike fermions and Higgs effective field theory revisited," *Phys. Rev. D* **96** no. 1, (2017) 015006, arXiv:1703.06134 [hep-ph].

[82] S.-P. He, "Leptoquark and vector-like quark extended model for simultaneousexplanation of W boson mass and muon g–2 anomalies*," *Chin. Phys. C* **47** no. 4, (2023) 043102, arXiv:2205.02088 [hep-ph].

[83] A. Arsenault, K. Y. Cingiloglu, and M. Frank, "Vacuum stability in the Standard Model with vectorlike fermions," *Phys. Rev. D* **107** no. 3, (2023) 036018, arXiv:2207.10332 [hep-ph]. 8

[84] **Particle Data Group** Collaboration, R. L. Workman *et al.*, "Review of Particle Physics," *PTEP* **2022** (2022) 083C01. 9, 10, 19

[85] A. Alloul, N. D. Christensen, C. Degrande, C. Duhr, and B. Fuks, "FeynRules 2.0 - A complete toolbox for tree-level phenomenology," *Comput. Phys. Commun.* **185** (2014) 2250–2300, arXiv:1310.1921 [hep-ph]. 9

[86] J. Alwall, R. Frederix, S. Frixione, V. Hirschi, F. Maltoni, O. Mattelaer, H. S. Shao, T. Stelzer, P. Torrielli, and M. Zaro, "The automated computation of tree-level and next-to-leading order differential cross sections, and their matching to parton shower simulations," *JHEP* **07** (2014) 079, arXiv:1405.0301 [hep-ph]. 9

[87] **NNPDF** Collaboration, R. D. Ball *et al.*, "Parton distributions from high-precision collider data," *Eur. Phys. J. C* **77** no. 10, (2017) 663, arXiv:1706.00428 [hep-ph]. 9

[88] J. Alwall, R. Frederix, S. Frixione, V. Hirschi, F. Maltoni, O. Mattelaer, H. S. Shao, T. Stelzer, P. Torrielli, and M. Zaro, "What are the default dynamic factorization and renormalization scales in madevent?" 2011. https://cp3.irmp.ucl.ac.be/projects/madgraph/wiki/FAQ-General-13. Accessed on 2023-12-25. 10

[89] **DELPHES 3** Collaboration, J. de Favereau, C. Delaere, P. Demin, A. Giammanco, V. Lemaître, A. Mertens, and M. Selvaggi, "DELPHES 3, A modular framework for fast simulation of a generic collider experiment," *JHEP* **02** (2014) 057, arXiv:1307.6346 [hep-ex]. 10

[90] **CERN** Collaboration, M. Selvaggi, "Delphes cards for LHC Run-III, HL-LHC and HE-LHC." December 6th, 2017. https://github.com/delphes/delphes/blob/master/cards/delphes_card_HLLHC.tcl. Accessed on 2023-12-25. 10

[91] **CERN** Collaboration, M. Selvaggi, "Delphes card for FCC-hh." October 14th, 2020. https://github.com/delphes/delphes/blob/master/cards/FCC/FCChh.tcl. Accessed on 2023-12-25. 10

[92] M. Cacciari, G. P. Salam, and G. Soyez, "FastJet User Manual," *Eur. Phys. J. C* **72** (2012) 1896, arXiv:1111.6097 [hep-ph]. 10

[93] M. Cacciari and G. P. Salam, "Dispelling the N^3 myth for the k_t jet-finder," *Phys. Lett. B* **641** (2006) 57–61, arXiv:hep-ph/0512210. 10

[94] E. Conte, B. Fuks, and G. Serret, "MadAnalysis 5, A User-Friendly Framework for

Collider Phenomenology," *Comput. Phys. Commun.* **184** (2013) 222–256, arXiv:1206.1599 [hep-ph]. 10

[95] L. Shang and Y. Zhang, "EasyScan_HEP: A tool for connecting programs to scan the parameter space of physics models," *Comput. Phys. Commun.* **296** (2024) 109027, arXiv:2304.03636 [hep-ph]. 10

[96] G. Cowan, K. Cranmer, E. Gross, and O. Vitells, "Asymptotic formulae for likelihood-based tests of new physics," *Eur. Phys. J. C* **71** (2011) 1554, arXiv:1007.1727 [physics.data-an]. [Erratum: Eur.Phys.J.C 73, 2501 (2013)]. 10

[97] N. Kumar and S. P. Martin, "Vectorlike Leptons at the Large Hadron Collider," *Phys. Rev. D* **92** no. 11, (2015) 115018, arXiv:1510.03456 [hep-ph]. 10